# A high performance memristor device and its filter circuit application

Chao Gao,[1] Hong Wang,[1] Zhiping Zhu,[1] Lei Zhang,[1] Yongqiang Yang,[3] Gang Cao,[1] Xiaobing Yan[1,2*]

[1]Key Laboratory of brain-like neuromorphic devices and Systems of Hebei Province, College of Electron and Information Engineering, Hebei University, Baoding, 071002, China

[2]Department of Materials Science and Engineering, National University of Singapore, Singapore, 117576, Singapore

[3]Jiangsu Province Special Equipment Safety Supervision and Inspection Institute, Branch of Wuxi, National Quality Supervision and Inspection Center of Graphene Products (Jiangsu), Wuxi 214174, P. R. China

[*] Corresponding author (email: yanxiaobing@ime.ac.cn or xiaobing_yan@126.com)

## Abstract

With the onset of big data era, memristors have been extensively studied for applications in nonvolatile neuromorphic computing owing to its fast switching speed and low switching power ability and CMOS compatibility. In particular, its adjustable cutoff frequency for filtering applications is a significant advantage. However, for circuit applications, memristors are still in their early simulated stage. In this study, Ag/$HfO_2$/graphene oxide quantum dots (GOQDs)/Pt structure memristor devices was fabricated, and GOQDs was used as a stability boost, with the bio-synapse simulation achieved and numerical recognition performed at an accuracy of 90.91%. A circuit-based filter was designed based on the memristor and STM32 microcontroller chip controlling, in which low-pass, high-pass, and band-pass filter circuits were all realized. By changing the output signal of the control circuit of the resistance value of the memristor, the cutoff frequency of the filter was successfully adjusted. This work therefore, paves a new way to obtain filter circuit application field of memristor for electronic system, and the overall performance of GOQDs inserted memristor was further optimized and its function in filtering realized, creating opportunities for further application of memristor in information processing.



This article has been accepted for publication and undergone full peer review but has not been through the copyediting, typesetting, pagination and proofreading process, which may lead to differences between this version and the Version of Record. Please cite this article as doi: 10.1002/pssr.202000389.

## 1. Introduction

Since after Chua has defined memristor's fourth circuit component in 1971,[1] it has been widely studied in nonvolatile memory, logic circuits,[2,3] neuromorphic computing[4,5] due to its advantages such as lossless readout, low power consumption, simple structure, and high data storage density.[6–8] However, there is an attendant challenge owing to non-uniform resistive switching (RS) parameters during increasing cycles for memristors, typically associated with the random nucleation and uncontrolled growth of conductive filaments (CFs) over a wide-area memory cell. If the position of the CF formation is restricted to specific regions in the memory cell, the stability of switching parameters will improve. Recently, numerous researches have focused on modulating the graphene size to below 100 nm, which is referred to as graphene oxide quantum dots (GOQDs).[9–12] GOQDs function as novel materials, as indicated in the field of memristors research,[13–17] and can boost the uniform distribution of SET and RESET voltages, robust retention, fast switching speed and low switching power and also increase the high–low resistance ratio.

However, due to its uniqueness, memristor creates a new challenge in the filter circuit design, and thus poses an attractive topic for researchers and engineers. Memristor have been investigated by numerous scientists for possible application in information processing.[18–20] Some memristor emulators have been reported in previous studies.[21] Filter was invented by Campbell and Wagner in 1917[22] and played important roles in many applications, such as image processing,[23] computer vision,[24,25] communication technology,[26] and time-frequency analysis.[27] In the traditional analog filter circuit, to realize adjustable cutoff frequency, the resistance in the circuit is usually replaced by the potentiometer, and the filter circuit cutoff frequency is changed by varying the resistance value of the potentiometer. Presently, most potentiometers are mainly analog mechanical and digital potentiometers, and because the stability of the mechanical potentiometer is not high, automatic control becomes challenging to realize. The resistance of the digital potentiometer is a discrete value and has a narrow pass band, which significantly affects the analog filter's accuracy and stability. For memristors, the resistance value has the characteristics of continuous change; thus the precision of memristors is higher than that of the digital potentiometer. The filter circuit structure based on the memristor device design is simple, in which its resistance control signal is pulse voltage, so it is easier to control and adjust the resistance value of the memristor than the programmable digital potentiometer. And then get the controllable, adjustable filtering circuit of the cut-off frequency.

In this study, 100-mesh GOQDs were inserted between the $HfO_2$ and Pt layers and Ag/$HfO_2$/GOQDs/Pt structure devices was constructed. Embedding the GOQDs greatly improved the uniformity and holding performance of the RS parameters, such as the reduction of threshold voltage, increasing the switching speed, and a high resistance ratio between high and low resistance states. When 500 pulses with ±0.6 V voltage and 200-ns pulse width are applied onto the memristor device, the conductance can be gradually adjusted. The memristor was also used as a digital recognition technology, and the accuracy rate was 90.91% for the 500$^{th}$ training. The filter circuits were designed and made into physical objects to realize low-pass, high-pass, and band-pass filtering applications, and consider high-pass filter as an example, the adjustable range of cutoff frequency is $f_c \in (0.16 \sim 1.429\text{GHz})$.

## 2. Results and Discussion

The schematic structure of the device is shown in Fig. 1(a), which demonstrates the components and processes of the device. A voltage bias is applied to the electrodes and a platinum (Pt) bottom electrode is used as the earthing during the electrical measurements. To distinguish the films' surface morphology, the atomic force microscopy (AFM) was used. Fig. 1(b) illustrates the surface topography of the pure-100 mesh GOQDs thin film. Before device fabrication, Raman were employed to characterize the 100-mesh GOQDs film are shown in Fig. 1(c).

Fig. 1(d) shows a series of electrical measurements on the device to confirm excellent electrical properties after with 100-mesh GOQDs. Statistically, current–voltage (I–V) curves were generated from overall 50 devices from two different batches, and 25 devices were randomly selected for each batch sample. Results showed that the device with 100-mesh GOQDs clearly exhibited outstanding repeatability under direct current (DC) voltage sweeping mode. The SET and RESET threshold voltages for the device were approximately 0.15 and −0.13 V, respectively. Further, the power consumption was compared with that of other devices (Fig. 1(e)), such as Without GOQDs, $MoSe_2$ QDs, RGO, and $MoS_2$.[28–30] Among these devices, the device with 100-mesh GOQDs displayed the lowest power consumption, which is advantageous to practical applications. To study the uniformity of RS memristor devices (MDs) further, the switching voltage distribution of 100-mesh GOQDs was analyzed, and from the analysis in Fig. 1(d), the SET and RESET voltage histogram of the memristor was calculated and the Gaussian fitting of each histogram is shown in Fig. S1(a-b) (see supplemental information), describing that the SET and RESET values of the 100 mesh GOQDs were limited to 0.11–0.16 V and -0.15– -0.11 V, respectively. Thus, the threshold voltage range of the device is obviously very narrow. In order to further describe the device with embedded GOQD showing higher stability, we have explained device mechanism model as shown in Fig. S2 (see supplemental information).

The switching speed between high and low impedance states is also a considerable parameter in memory cell applications. This plays a key role in circuit design. Therefore, the switching speed of two devices was subsequently investigated. To turn the device on and off with 100-mesh GOQDs, 2 V positive pulse and −2 V negative pulse with 120 and 150-ns widths, respectively, were used, as shown in Fig. S1(c-d) (see supplemental information). We observed that the device can successfully function. Further, these devices can be programmed to LRS and HRS at pulse widths of approximately 7 and 25 ns (see supplemental information Fig. S1c-d), respectively, in programming operations, indicative of a faster switching speed compared with conventional RRAM.[31,32] Fig. 1(f) shows that the 100-mesh GOQDs exhibited stable RS over 200 cycles with on/off ratio of ~1M. In addition, we tested the device, which shows good retention properties at 70 °C. The results are shown in Fig. S3 (see supplemental information).

Fig. 1(g) illustrates the I–V characteristics of 40 points in the device, with an average resistance of 80 MΩ and 230 Ω for HRS and LRS at 0.05V, respectively, and an average on–off ratio of 0.35 M. For LRS and HRS with a resistance of 100 Ω and 100MΩ respectively, the maximum on–off ratio is 1 M. The impact of pulse parameters (e.g., pulse amplitude) on the resistance modulation via the migration of Ag ions under an electrical field in single voltage polarity is identical to the behavior of bio-synapses. Owing to the extremely fast response time of the device, nanosecond bidirectional pulses with positive and negative polarities were used to tune the device condition in detail. Studies on the influence of the amplitude of the pulse train on the resistance variation were conducted when sustained train spikes was used in the memristor cell. Furthermore, the width and interval of each pulse were 60 and 90 ns, respectively. The dependence of MD resistance on the positive and negative pulse amplitudes is shown in Fig. 1(h) and (i), respectively. The resistance varied faster with the increase of both positive and negative pulse amplitudes, respectively.

Neural networks can perform computational tasks such as image and pattern recognition, or filter circuit after learning using a training dataset. The synaptic plasticity, i.e., the capability of a synapse to modulate its weight in response to the signals it transmits between neurons, establishes the encoding of neuronal inputs. Short-term potentiation refers to fast and reversible changes in the synaptic weight, and it is essential for brain functions like pattern recognition, associative learning, and sound localization.[33,34] However, long-term potentiation (LTP) denotes a more persistent increase in the synaptic weight, leading to long-lasting modifications in neuronal signal transmissions. This approach resembles long-term memory in biological systems. Recent works have shown the use of oxide filamentary resistance switching devices and phase change memories with unsupervised learning identical to biological neural networks.[35-39] Positive/negative bidirectional pulse sequences for different parameters to stimulate synapses and related tests of spike-timing-dependent plasticity, see Fig. S4(a) (see supplemental information).

An essential condition for memristors in artificial neural networks is a controlled access to a large number of distinct conductance states. In Fig. 2(a–c), the control over the junction conductance using trains of writing pulses with fixed amplitude is shown. Here, the differences between voltage pulses that are too small and are too large to trigger complete polarization reversal are been determined. The voltage of ± 0.6 V, as shown in Fig. 2(c), was chosen. If the voltage pulse is such that it will operate in a single direction, it will switch its own conductance state at a voltage of ± 0.6 V, as shown in Fig. 2(a) and (b). Fig. 2(a) and (b) indicate that under these conditions, the junction conductance continuously varies up to 500 writing pulses with the duration time interval of 200 ns each. The potentiation (Fig. 2(a)) and depression (Fig. 2(b)) during uninterrupted signaling follow a second-order exponential growth and decay function (red lines), respectively. An essential characteristic of cognitive learning is the more pronounced change of synaptic weight during the early stages of activation, which has also been realized using metal-oxide memristors.[40] The total variation of conductance is larger for the positive pulse (+0.6 V) state, at above 100%, against an effect of −92.3% for the negative pulse(−0.6 V) state.

In addition, the following task was conducted using digital recognition by memristor. At present, various neural networks based on memristor have been proved to have higher energy efficiency in the field of pattern recognition.[41] In this section, we use back propagation algorithm to recognizing handwritten digits 0-9 in the Modified National Institute of Standards and Technology (MNIST) database with artificial neural network (ANN) based on memristive artificial synapse.[42] In this ANN structure, 10 output nodes represent 10 results (0-9) in the MNIST dataset, and a 28 × 28 pixel sample corresponds to 784 input nodes. The first output $V_{out}$#1 is a controllable voltage signal of ANN, which will lead to the corresponding artificial synapse to produce higher synaptic weight than other nodes. Therefore, in Fig. 2d, the recognition of "0" is realized. The weighted parameter map more clearly reflects the recognition of the numbers 0-9 after training. After 50 trainings, a 73.96% accuracy rate of digit recognition was obtained, and after 500 trainings, a digit recognition accuracy rate of 90.91% was obtained (Fig. 2e-g). Compared with Kim's work,[43] under the same accuracy, our proposed memristor device allows to work at lower voltage amplitudes and shorter pulse widths and intervals.

The synaptic efficacy in the nervous systems can significantly increase (synaptic facilitation) or decrease (synaptic depression) within milliseconds after the onset of specific temporal patterns of activity.[44] Owing to the short-term synaptic depression or facilitation, synapses can also function as dynamic filters for information transmission based on signal frequencies.[45] The short-term synaptic depression and facilitation contribute to low-pass and high-pass temporal filtering, respectively. As different Δt in our 100-mesh GOQDs synaptic transistor can get different paired-pulse facilitation index and the variation is large, the filter could be realized, see Fig. S4(b) (see supplemental information). Important synaptic dynamic functions, like excitatory postsynaptic current (EPSC), were satisfactorily mimicked. Fig. 3(a) demonstrates the EPSC responses of our device to the stimulus train with varying frequencies. The stimulus train at each frequency comprises 10 stimulus spikes (+0.6 V, 200 ns). The first one is called A1, and the tenth is called A10. The peak value of the EPSC is 0.34 mA after 10 spikes for 200 kHz frequency of the stimulus train. Upon increasing the frequency of the stimulus train, the peak values of the EPSCs also increase. Fig. 3(b) illustrates the frequency-dependent gain determined as the ratio of the amplitudes between tenth EPSC (A10) and first EPSC (A1). The gain increases from 2.2 to 12.2 when the stimulus frequency changes from 200 kHz to 2000 kHz, denoting that the synaptic transistor can function as a dynamic filter for information transmission. The temporal filtering mimicked herein is useful for neuromorphic computations or artificial neural networks.

A filter is a frequency selective circuit that allows signals in one frequency range to pass through and has a greater inhibitory effect on signals in other frequency ranges. In the filter circuit, the frequency range that the signal is not suppressed is called the passband, while the frequency range that the signal has great attenuation or even is completely suppressed is called the stop-band, and the cutoff point between the stop-band and the passband is called the cutoff frequency. According to the frequency range, it can be divided into high-pass, low-pass, band-stop, and band-pass filters.

The filter circuit composed of resistance, capacitance, and inductance is the most widely used in analog filters. In a traditional filter, once the structure of the circuit, resistance, capacitance, and inductance are determined, the passband and cutoff frequency of the filter cannot be changed.

In order to realize the adjustable cutoff frequency, we designed a filter circuit based on the 100-mesh GOQDs memristor. In this filter circuit, when the voltage applied to both ends of the memristor is higher than the threshold voltage, the memristor's resistance value changes; otherwise, the memristor's resistance value remains unchanged. Therefore, when the memristor works in a small signal analog circuit, the control signal whose amplitude is greater than the threshold voltage is used to vary the memristor's resistance value; hence, the cutoff frequency of the filter circuit can be adjusted.

The High-pass filter, low-pass and band-pass filters and the first order RC (resistance-capacitance) circuit are shown in Fig. S5(a-c) (see supplemental information). Considering a high-pass filter as an example, where the input signal is $V_i$ and the output signal is $V_o$. From Kirchhoff's voltage law and Laplace's law:

$$V_o = C\frac{dV_i}{dt}R - C\frac{dV_o}{dt}R \tag{1}$$

$L[V_i] = R(s)$; $L[V_o] = C(s)$, by taking the Laplace transform of the above equation, we can obtain:

$$C(s) = C \times R \times S \times (R(s)-C(s)) \tag{2}$$

$$G(s) = \frac{CRS}{1+CRS} \tag{3}$$

The type (3) $s = j\omega$, $\omega$ is the angular frequency of the input signal. Therefore, the transfer function $G(s)$ of the RC high-pass filter circuit is related to the frequency, resistance, and capacitance of the input signal. In this circuit, due to the constant resistance and capacitance, when the frequency changes, the transfer function of the circuit also changes, and the output signal $V_o$ of the circuit is significantly enhanced or suppressed, thus achieving the purpose of frequency selection.

Because the cutoff frequency of the filter circuit is $f_c = \frac{1}{2\ RC}$, the filter cutoff frequency can be adjusted by changing the resistance and capacitance, by replacing the capacitance and resistance with the memristor in a first order RC high-pass filter circuit as shown in Fig. S5(a) (see supplemental information), the memristor-based high-pass filter circuit is obtained as shown in Fig. 4a,[46] and a control circuit based on STMicroelectronics 32-bit series microcontroller chips (STM32) microcontroller can be obtained as shown in Fig. S6 (see supplemental information). The high-pass filter circuit was made into a real object for testing, as shown in Fig. 4(b). $R_{M1}$ and $R_{M2}$ are memristors. The $R_{M1}$ resistance value control circuit and $R_{M2}$ resistance value control circuit are used to control the resistance value of the memristor $R_{M1}$ and memristor $R_{M2}$ respectively, and the resistance can be continuously regulated. Take $R_{M1}$ as an example. When rm1a is of high level and rm1b is low level, the output of $R_{M1}$ resistance control circuit is $V_{pp}$. When rm1a is at a low level, rm1b is at a high voltage, $R_{M1}$ resistance value control circuit output for the $-V_{pp}$; $R_{M2}$ control method is the same as $R_{M1}$; Related parameters of the circuit is: $R_{M1}$ and $R_{M2}$ related parameters are based on low resistance $R_{on}$ = 100 Ω, high resistance $R_{off}$ = 100MΩ, initial resistance $R_{init}$ = 1MΩ, open voltage $V_T$ = 0.1 V, off voltage $V_R$ = −0.1 V; Control circuit $V_{pp}$ = 0.2 V; Capacitance C = 1 pF; Resistance $R_{C1} = R_{C2}$ = 10 Ω, R = 10000 Ω. According to,[46-48] high-pass filter circuit based on memristor can be equivalent to the R(t)C(t) circuit as shown in Fig. 4(c). Where variable resistance $R(t) = R_{C1} + R_{M1} + R$, variable capacitance $C(t) = (R_{C1}+R_{M2})C/R$. Therefore, in the high-pass filter circuit based on memristor, its cutoff frequency is:

$$f_c = \frac{1}{2\ R(t)C(t)} = \frac{R}{2\ (R_{C1}+R_{M1}+R)(R_{C2}+R_{M2})C} \tag{4}$$

According to formula (4), by changing the size of the variable resistance R(t) and the variable capacitance C(t) through the resistance value control circuit, the cutoff frequency of the low-pass filter circuit can be changed. A sinusoidal excitation signal is applied to the input of the filter circuit, and the amplitude of the excitation signal is less than the threshold voltage of the memristor. The amplitude–frequency and phase–frequency response curves of the circuit were obtained by Matlab, as shown in Fig. 4 (d).

Fig. 4 (d) demonstrates the amplitude–frequency and phase–frequency response curves of the memristor in high and low resistance states respectively, that is, the variation interval of the response curve is between the two curves as the resistance changes. The cutoff frequencies in the high and low resistance states are: $f_{c1}$ = 0.16H$_Z$，$f_{c2}$ = 1.429GH$_Z$，and the cutoff frequency can be controlled within the appeal range, i.e.,

$$f_c \in (0.16 \sim 1.429\text{GHz})$$

In addition, we divide the Fig. 5 into three rows and three columns. Sine waves of different frequencies were used as input, and the sine waves collected were shown in Fig. 5. According to the resistance changes reflected in Fig. 1 (h–i), three sets of data was measured by using the memristor-based high-pass filter circuit. The horizontal comparison reflected the comparison of output and input as the frequency increased. The longitudinal reflection is a comparison of three different impedance states. Where the second column corresponds to the cutoff frequencies of the three impedance states. The first line is measured when both $R_{M1}$ and $R_{M2}$ are $1 \times 10^4$ Ω. The second line is measured when both $R_{M1}$ and $R_{M2}$ are $1.5 \times 10^4$ Ω. The third line is measured when both $R_{M1}$ and $R_{M2}$ are $2 \times 10^4$ Ω. As the frequency increases, the output becomes closer and closer to the input sine wave. The high-pass filter with an adjustable cutoff frequency is realized.

**3. Conclusion**

In summary, we have designed a memristor by using 100-mesh GOQDs which performance has been greatly improved in electrical characteristics, biological synapse simulation, and the like. The resistance of memristor can be controlled and adjusted to realize the application of memristor in filter circuits. Filter circuits based on memristor perform excellent in high-pass, low-pass, and band-pass filters. This work created a new foundation for memristors in intelligent control and artificial intelligence.

**4. Experimental Section**

A simple interposed structure device was prepared via the magnetic sputtering and spin coating techniques. A layer of 100-mesh graphene was coated on a commercial platinum substrate by rotating and coating at 1500 RPM and drying it for 5 hours. Next, $HfO_2$ films having 15-nm thickness was deposited on a 100-mesh graphene quantum dot using the magnetron sputtering method at 3-Pa base pressure under the gas flow of 50-SCCM (cubic centimeter per minute at standard temperature and pressure) Ar and 25-SCCM $O_2$ mixed atmosphere. Subsequently, 50-nm-thick top Ag electrodes with 100-nm diameter were prepared using the direct current reactive magnetron sputtering process, and at last, the devices with Ag/$HfO_2$/GOQDs/Pt structure were prepared.

The electrical characteristics were measured in the atmospheric environment with a Keithley 4200 source-measure unit. An Agilent 33250A function/arbitrary waveform generator and lecroywaver-runner 62Xi oscilloscope were used to determine the endurance of memory cells.

**Acknowledgments**

This work was financially supported by the National Natural Science Foundation of China (grant nos. 61674050 and 61874158), the Outstanding Youth Project of Hebei Province (grant no. F2016201220), the Project of Distinguished Young of Hebei Province (grant no. A2018201231), the Support Program for the Top Young Talents of Hebei Province (grant no. 70280011807), the Training and Introduction of High-level Innovative Talents of Hebei University (grant no. 801260201300), the Hundred Persons Plan of Hebei Province (grant nos. E2018050004 and E2018050003), the 2020 School level Innovation Program of Hebei University (hbu2020ss001), and the Supporting Plan for 100 Excellent Innovative Talents in Colleges and Universities of Hebei Province (no. SLRC2019018).

**Conflict of Interest**

The authors declare no conflict of interest.

**Keywords**

Graphene oxide quantum dots; Memristor; Filter circuit

**References**

[1] L. O. Chua, IEEE Trans. on Circuit Theory. **1971**, 18, 507-519.

[2] X. B. Yan, Y. D. Xia, H. N. Xu, X. Gao, H. T. Li, R. Li, J. Yin and Z. G. Liu, Appl. Phys. Lett. **2015**, 97, 112101.

[3] A. Siemon, T. Breuer, N. Aslam, S. Ferch, W. Kim, J. D. Hurk, V. Rana, S. Hoffmann-Eifert, R. Waser, S. Menzel and E. Linn, Adv. Funct. Mater. **2015**, 25, 6414-6423.

[4] J. J. Yang, D. B. Strukov and D. R. Stewart, Nat. Nanotechnol. **2013**, 8, 13-24.

[5] T. Ohno, T. Hasegawa, T. Tsuruoka, K. Terabe, J.M. Gimzewski and M. Aono, Nat. Mater. **2011**, 10, 591-595.

[6] R. Waser, and M. Aono, Nat. Mater. **2007**, 6, 833-840.

[7] B. Cho, S. Song, Y. Ji, T.-W. Kim, and T. Lee, Adv. Funct. Mater. **2011**, 21, 2806-2829.

[8] M. D. Ventra, and Y.V. Pershin, Mater. Today. **2011**, 14, 584-591.

[9] S. Neubeck, L. A. Ponomarenko, F. Freitag, A. J. M. Giesbers, U. Zeitler, S. V. Morozov, P. Blake, A. K. Geim and K. S. Novoselov, Small. **2010**, 6, 1469-1473.

[10] S. Schumacher, Phys. Rev. B: Condens. Matter Mater. Phys. **2011**, 83, 081417.

[11] M. Li, W. B. Wu, W. C. Ren, H. Cheng, N. J. Tang, W. Zhong and Y. W. Du, Appl. Phys. Lett. **2012**, 101, 103107.

[12] N. Leconte, J. Moser, P. Ordejon, H. Tao, A. Lherbier, A. Bachtold, F. Alsina, C. M. S. Torres, J. C. Charlier and S. Roche, ACS Nano. **2010**, 4, 4033-4038.

[13] X. B. Yan, Z. Lei, Y. Q. Yang, Z. Y. Zhou, J. H. Zhao, Y. Y. Zhang, Q. Liu and J. S. Chen , Journal of Materials Chemistry C. **2017**, 5, 11046-11052.

[14] Y. Li, H. Shu, S. Wang and J. Wang, J. Phys. Chem. C. **2015**, 119, 4983-4989.

[15] R. L. Liu, D. Q. Wu and X. L. Feng, J. Am. Chem. Soc. **2011**, 133, 15221-15223.

[16] H. Y. Jeon, J. Y. Park, W. C. Jang, H. J. Kim, S. B. Ahn, K. Jeon, H. T. Seo and H. Jeon, Carbon. **2014**, 75, 209-216.

[17] H. Y. Jeong, O. J. Y. Kim, J. W. Kim, J. O. Hwang, J. Kim, J. Y. Lee, T. H. Yoon, B. J. Cho, S. O. Kim, R. S. Ruoff and S. Choi, Nano Lett. **2010**, 10, 4381-4386.

[18] M. Itoh and L. Chua, International Journal of Bifurcation and Chaos. **2009**, 19, 3605-3656.

[19] S. H. Jo, T. Chang, I. Ebong, B. B. Bhadviya, P. Mazumder, and W. Lu, Nano Letters. **2010**, 10, 1297-1301.

[20] Q. F. Xia, W. Robinett, M. W. Cumbie, N. Banerjee, T. J. Cardinali, J. J. Yang, W. Wu, X. Li, W. M. Tong, D. B. Strukov, G. S. Snider, G. Medeiros-Ribeiro, and R. S. Williams, Nano Letters. **2009**, 3640-3645.

[21] P. S. Maheshwar, Y. Changju, K. Hyongsuk, and C. Leon, Sensors. **2012**, 12, 3587-3604.

[22] L. Campbel, and A. George, Bell System Technical Journal. **1922**, 1, 1-32.

[23] K. D. Baker, and G. D. Sullivan, IEE Proceedings E-Computers and Digital Techniques. **1980**, 127, 173-184.

[24] P. Luciano, C. L. Sotiropoulou, S. Gkaitatzis, M. Viti, S. Citraro, A. Retico, P. Giannetti, and M. Dell'Orso, IEEE Trans. on Nuclear Science. **2017**, 64, 1374-1381.

[25] Z. Zhang, and K. H. Wong, Electronics and Computer Engineering. **2013**, 188-193.

[26] I. Steiner, and G. A. Jullien, Systems and Computers. IEEE. **2007**, 2009-2013.

[27] X. C. Niu, X. G. Wu, P. Xie, and L. Pan, Proc. of the 11thWorld Congress on IEEE Intelligent Control and Automation. **2014**, 5179-5184.

[28] X. B. Yan, Y. F. Pei, H. W. Chen, J. H. Zhao, Z. Y. Zhou, H. Wang, L. Zhang, J. J. Wang, X. Y. Li, Z. A. Xiao, Q. L. Zhao, K. Y. Wang, H. Li, D. L. Ren, Q. Liu, H. Zhou, J. S. Chen, and P. Zhou, Advanced materials. **2019**, 31, 1805284.

[29] S. K. Pradhan, B. Xiao, S. Mishra, A. Killam and A. K. Pradhan, Sci. Rep. **2016**, 6, 26763.

[30] P. Zhang, C. X. Gao, B. H. Xu, L. Qi, C. J. Jiang, M. Z. Gao and D. S. Xue, Small. **2016**, 15, 2077-2084.

[31] N. Xu, L. F. Liu, X. Sun, C. Chen, Y.Wang, D. D. Han, X. Y. Liu, R. Q. Han, J. F. Kang and B. Yu, Semicond. Sci. Technol. **2008**, 23, 075019.

[32] L. J. Zhang, R. Huang, M. H. Zhu, S. Q. Qin, Y. B. Kuang, D. J. Gao, C. Y. Shi and Y. Y. Wang, IEEE Electron Device Lett. **2010**, 31, 966-968.

[33] E. S. Fortune and G. J. Rose, Trends Neurosci. **2001**, 24, 381-385.

[34] R. S. Zucker and W. G. Regehr, Annu. Rev. Physiol. **2002**, 64, 355-405.

[35] A. Serb, J. Bill, A. Khiat, R. Berdan, R. Legenstein and T. Prodromakis, Nat.Commun. **2016**, 7, 1-9.

[36] Z. Wang, S. Joshi, S. Savel' ev, W. Song, R. Midya, Y. Li, M. Rao, P. Yan, S. Asapu, Y. Zhuo, H. Jiang, P. Lin, C. Li, J. H. Yoon, N. K. Upadhyay, J. Zhang, M. Hu, J. P. Strachan, M. Barnell, Q. Wu, H. Wu, R. S. Williams, Q. Xia and J. J. Yang, Nat. Electron. **2018**, 1, 137-145.

[37] I. Boybat, M. Le Gallo, S. R. Nandakumar, T. Moraitis, T. Parnell, T. Tuma, B. Rajendran, Y. Leblebici, A. Sebastian and E. Eleftheriou, Nat. Commun. **2018**, 9, 1-12.

[38] V. Milo, G. Pedretti, M. Laudato, A. Bricalli, E. Ambrosi, S. Bianchi, E. Chicca, D. Ielmini, presented at IEEE Int. Symp. Circuits Syst. (ISCAS), **2018,** 1-5.

[39] M. Lanza, H.-S. Philip Wong, E. Pop, D. Lelmini, D. Strukov, B. C. Regan, L. Larcher, M. A. Villena, J. J.

Yang, L. Goux, A. Belmonte, Y. Yang, F. M. Puglisi, J. Kang, B. Magyari-Köpe, E. Yalon, A. Kenyon, M. Buckwell, A. Mehonic, A. Shluger, H. Li, T.-H. Hou, B. Hudec, D. Akinwande, R. Ge, S. Ambrogio, J. B. Roldan, E. Miranda, J. Suñe, K. L. Pey, X. Wu, N. Raghavan, E. Wu, W. D. Lu, G. Navarro, W. Zhang, H. Wu, R. Li, A. Holleitner, U. Wurstbauer, M. C. Lemme, M. Liu, S. Long, Q. Liu, H. Lv, A. Padovani, P. Pavan, I. Valov, X. Jing, T. Han, K. Zhu, S. Chen, F. Hui and Y. Shi, Adv. Electron. Mater. **2018**, 1800143.

[40] I. Gupta, A. Serb, A. Khiat, R. Zeitler, S. Vassanelli and T. Prodromakis, Nat. Commun. **2016**, 7, 1-9.

[41] X. B. Yan, C. Y. Qin and C. Lu, ACS Applied Materials & Interfaces. **2019**, 11, 48029-48038.

[42] S. Choi, S. H. Tan, Z. Li, Y. Kim, C. Choi, P.-Y. Chen, H. Yeon, S. Yu and J. Kim, Nat. Mater. **2018**, 17, 335-340.

[43] H. Kim, S. Hwang, J. Park and B. Park, Nanotechnology. **2017**, 28, 405202.

[44] E. S. Fortune, and G. J. Rose, Trends Neurosci. **2001**, 24, 381-385.

[45] L. F. Abbott, and W. G. Regehr, Nature. **2004**, 431, 796-803.

[46] M. D. Ventra, Y. V. Pershin and L. O. Chua, Proceedings of the IEEE. **2009**, 97, 1717-1724.

[47] Y. V. Pershin and M. D. Ventra, IEEE Transactions on Circuits and System I: Regular Papers. **2010**, 57, 1857-1864.

[48] Y. V. Pershin and M. D. Ventra, Electronics Letters, April. **2010**, 1, 517-518.

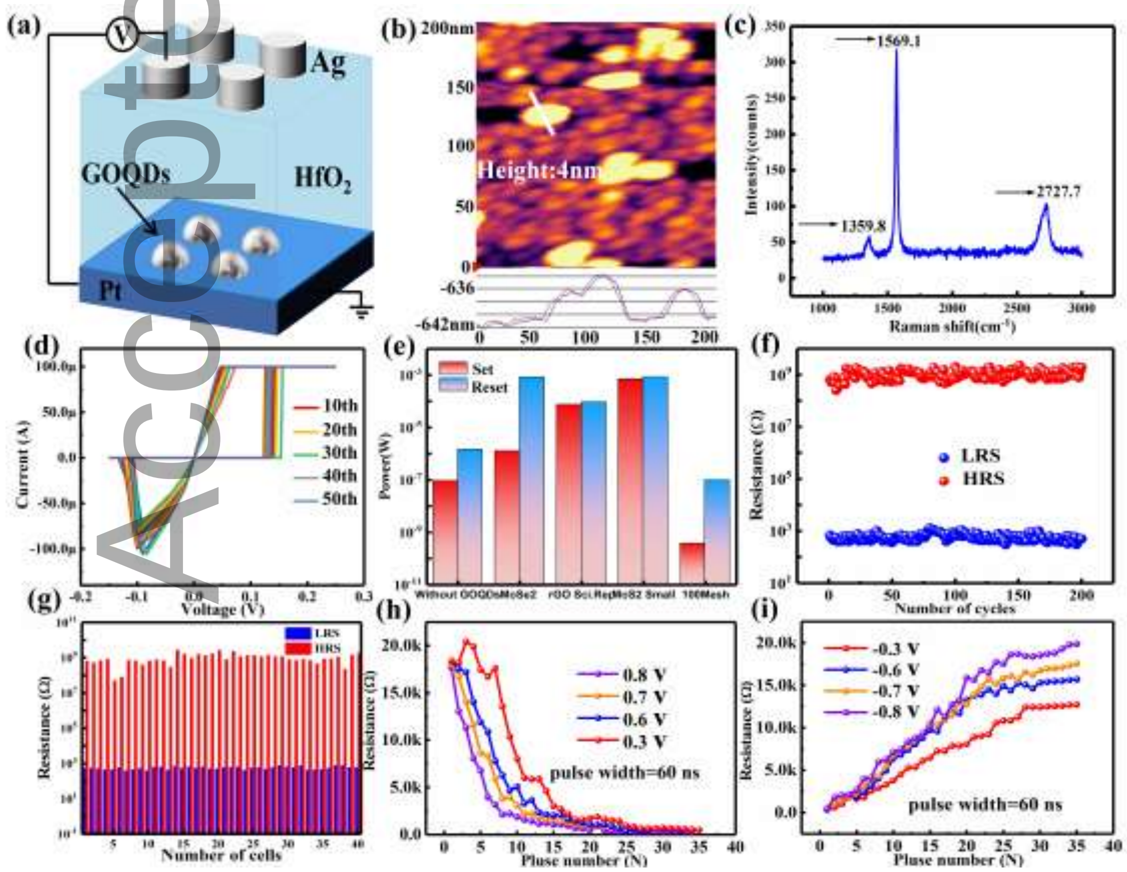


**Figure 1.** (a) A schematic of an electrical measurement device that characterizes an

Ag/$HfO_2$/GOQDs/Pt device with 100-mesh graphene oxide quantum dots inserted. Microscopic characteristics: (b) AFM image of the 100-mesh GOQDs on the Pt. (c) Raman spectrum of 100-mesh GOQDs. (d) Ag/$HfO_2$/GOQDs/Pt current–voltage (I–V) curve with 100-mesh graphene oxide quantum dots inserted. (e) Comparison of equipment power and literature values. (f) Endurance of 100-mesh GOQDs based memristors determined with writing and erasing voltages of 0.1 and −0.1 V, respectively. The pulse width was 200ns. (g) HRS and LRS of 40 cells measured for data reliability at 0.05 V. Positive/negative bidirectional pulse trains for exciting/inhibiting the synapse with different parameters were also measured. (h-i) Impact of the positive/negative pulse train amplitudes on the resistance modulation.



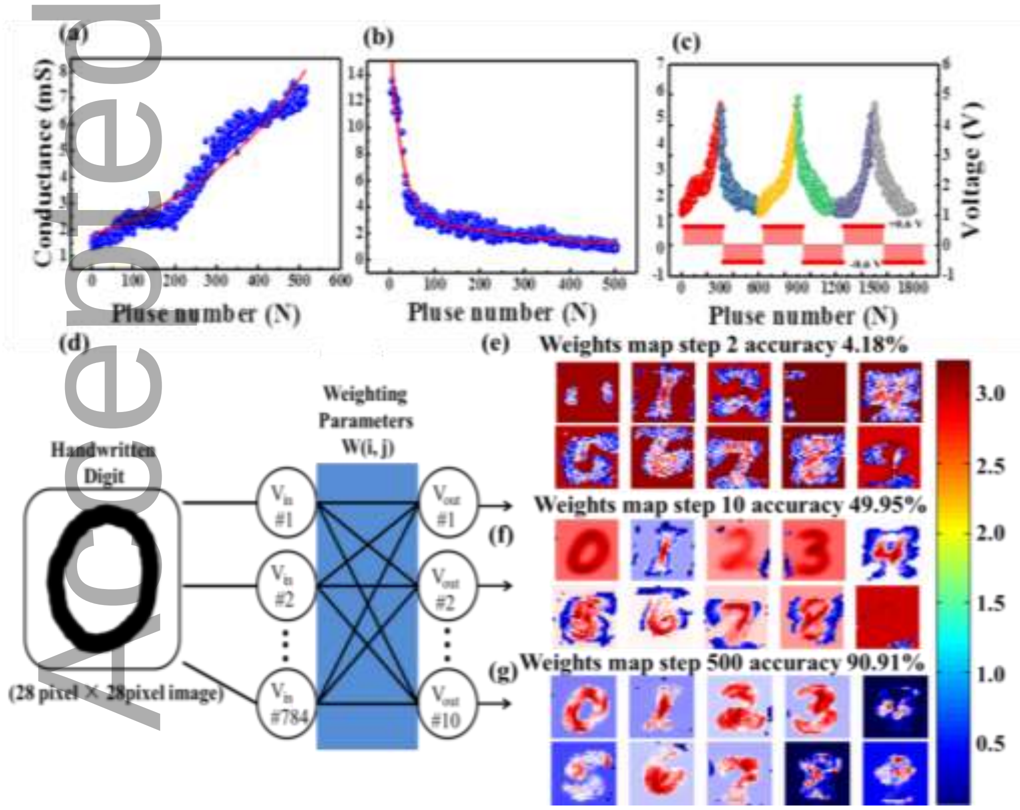


**Figure 2.** Pulse regulation. Modulation of junction conductance using pulse amplitude and number. (a, b) Variation of junction conductance during continuous activation using a train of 500 identical voltage pulses. The interval between pulses is 200 ns and their amplitude is +0.6 V in (a) and −0.6 V in (b). The red lines are fits to Double exponential attenuation fitting functions of y = $A_1$×exp

$(-x/t_1) + A_2 \times \exp(-x/t_2) + y_0$. (c) Conductance variation for pulse trains with small alternating amplitudes of +0.6 and −0.6 V. (d) The single-layer architecture of ANN systems. When an input digit image is 0, the top-right neuron $V_{out}$#1 will fire. (e-g) The relationship between different training time and accuracy. (e) The map of weighting parameters posts 2 training iterations, which corresponds to a digit recognition accuracy of 4.18%. (f) The map of weighting parameters posts 10 training iterations, which corresponds to a digit recognition accuracy of 49.95%. (g) The map of weighting parameters posts 500 training iterations, which corresponds to a digit recognition accuracy of 90.91%.



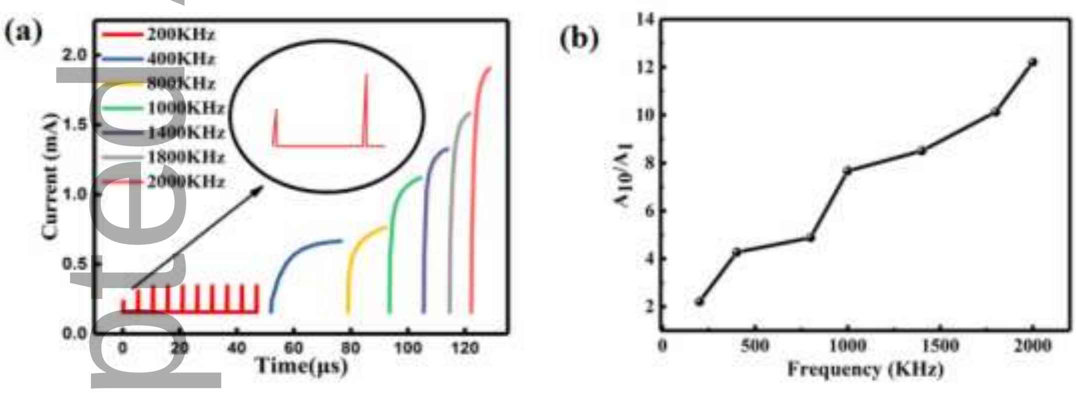


**Figure 3.** (a) Excitatory postsynaptic currents (EPSC) recorded in response to the stimulus train with varying frequencies. The stimulus train at each frequency comprises 10 stimulus spikes (+0.6 V, 200 ns). (b) EPSCs amplitude gain (A10/A1) plotted as a function of presynaptic spike frequency.

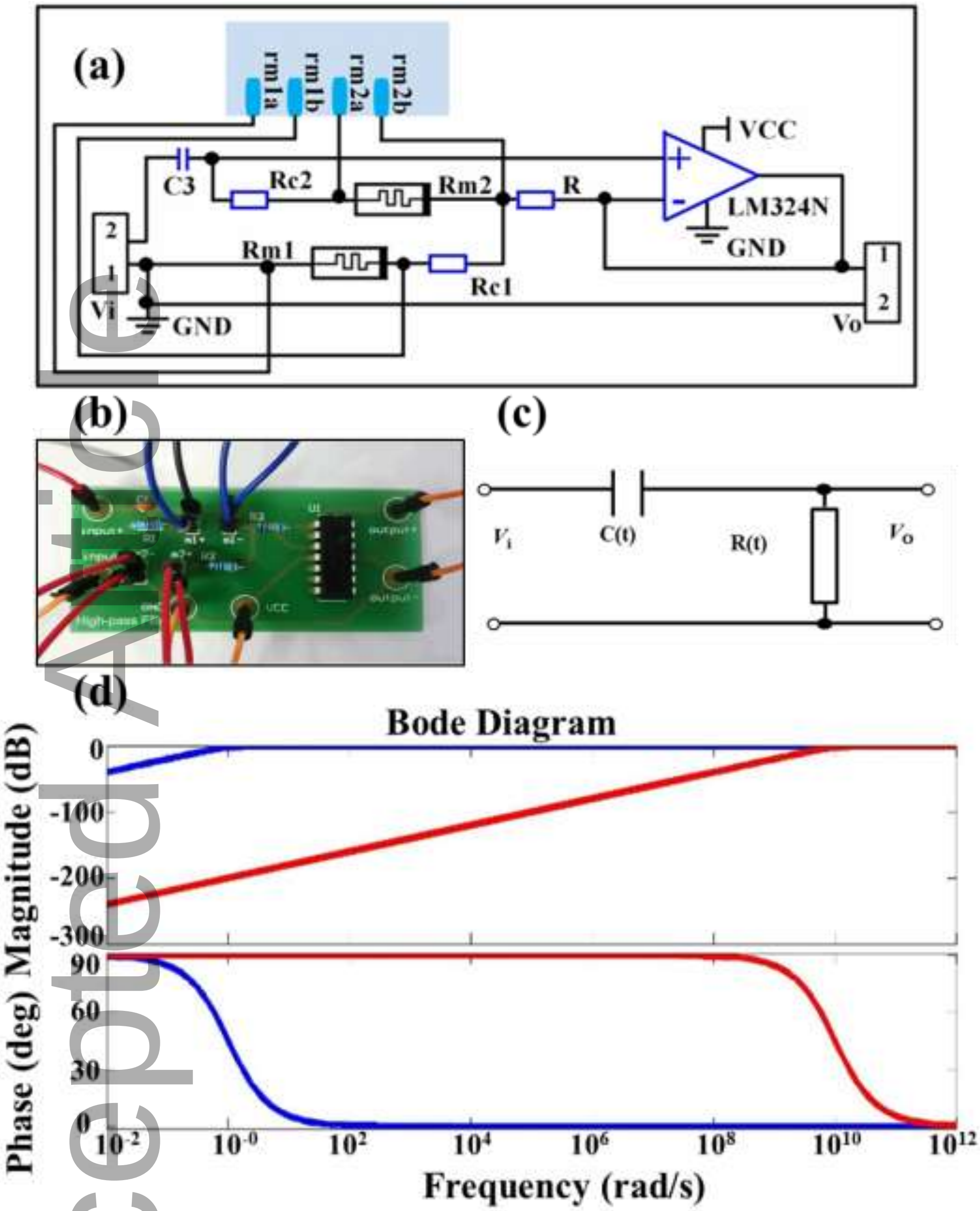


**Figure 4.** (a) High-pass filter circuit based on memristor. (b) Physical map of filter circuit based on 100-mesh GOQDs memristor. (c) The equivalent circuit of a high-pass filter circuit. (d) Response curves of amplitude–frequency and phase–frequency of the high-pass filter circuit.

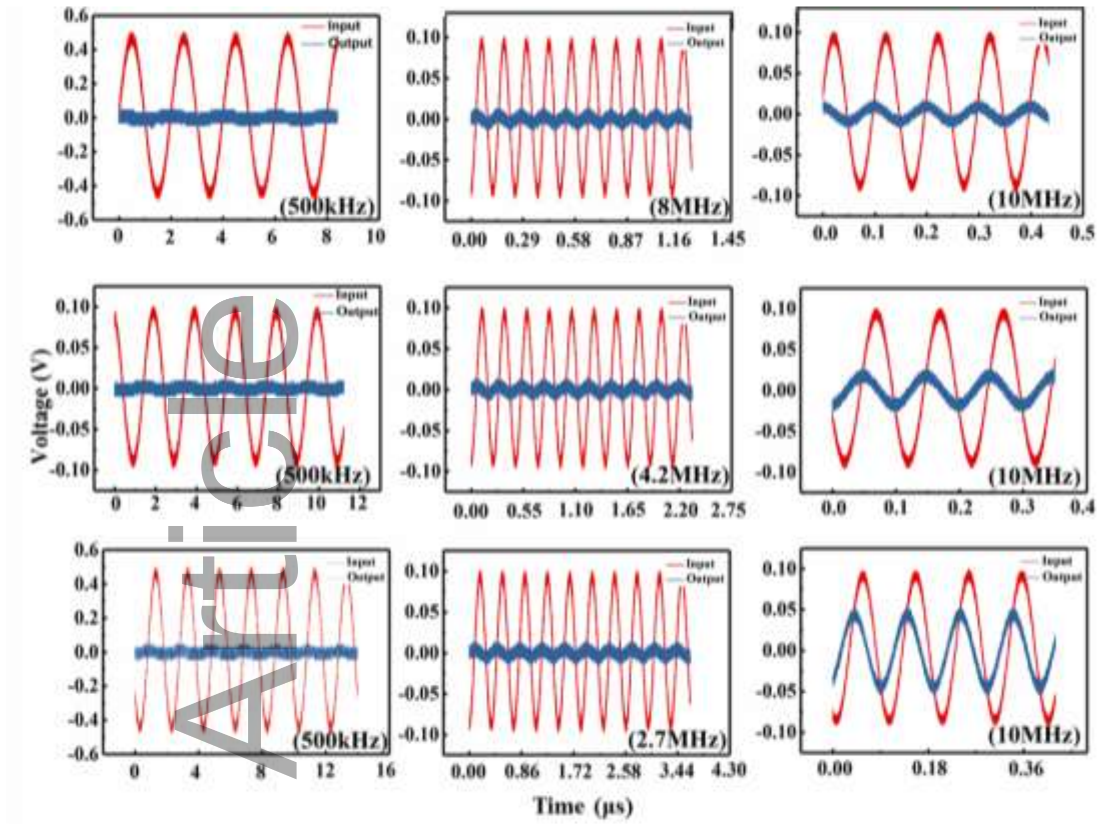


**Figure 5.** The output of the high-pass filter shows the input sine wave (red) and output sine wave (blue) shapes.

## The Table of Contents

The $Ag/HfO_2/GOQDs/Pt$ memristor have more concentrated SET and RESET voltage distribution, and the resistance of memristor can be controlled and adjusted, which can realize the application of memristor in filter circuits.

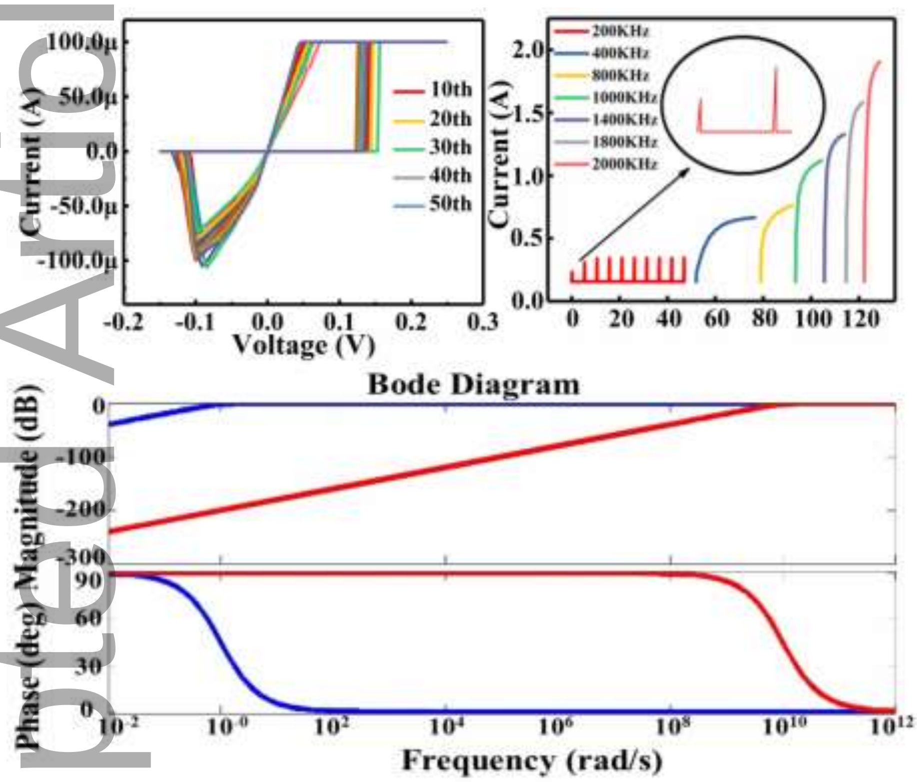


ToC Figure